Quantitative Analysis of Knee Movement Patterns through Comparative Visualization

Khoa Tan Nguyen[a], Håkan Gauffin[b], Anders Ynnerman[a], Timo Ropinski[a]

[a]*Scientific Visualization Group, Linköping University, Sweden*
[b]*Orthopedic Department, Linköping University Hospital, Sweden*

Abstract

In this paper, we present a novel visualization approach for the quantitative analysis of knee movement patterns in time-varying data sets. The presented approach has been developed for the analysis of patello-femoral instability, which is a common knee problem, caused by the abnormal movement of the patella (kneecap). Currently, patello-femoral analysis is based on acquisitions performed during a 30 or 45 degrees of knee flexion, which is analyzed in so-called Skyline or Merchant views. Because of the limited range of considered knee flexions, this technique does not adequately reveal the instability of the kneecap at full extension. While 3D imaging of the straight knee can help to improve the diagnostic process, its static nature does not permit the analysis of the dynamics of the patellar under functional movements. Recently, 4D CT imaging has become available as a new modality for kinetic joint movement analysis. The inclusion of the time domain in 4D CT scans enables the acquisition of the kinematic behavior of joints under natural conditions. However, quantitative analysis on such 4D CT scans is challenging. Our approach investigates the quantitative kinematic analysis of complex joint movements in time series data. By supporting the ability to track features of interest (FOIs) in the time domain, the quantitative analysis process can be facilitated in a semi-automatic manner. Moreover, it allows us to visualize the movement of the patellar in the femoral groove during an active flexion and extension movement, which is essential to assess kinematics with respect to knee flexions. To further support quantitative analysis, we propose kinematic plots and time-angle profiles, which enable comparative dynamics visualization. As a result, our proposed visualization approach facilitates better understanding of the effects of surgical interventions by quantifying and comparing the dynamics before and after the operations. We demonstrate our approach using clinical time-varying patello-femoral data, discuss its benefits with respect to quantification as well as medical reporting, and describe how to generalize it to other complex joint movements.

Keywords: 4D CT, quantitative analysis, feature identification and matching

Email address: tan.khoa.nguyen@liu.se (Khoa Tan Nguyen)

1. Introduction

As the major focus of medical imaging has been the understanding of anatomical structures, vast research effort has been dedicated to the acquisition and interpretation of anatomical modalities. While these techniques enable the interpretation of high-resolution static anatomical images, time-varying data is now becoming more important. The better understanding of organ functions can provide more insight and significantly improve the diagnostic workflow. This has led to the emergence of many functional modalities, which allow multimodal imaging of physiological processes alongside the anatomical image data serving as a context. The latest exploitation of anatomical modalities in a functional context arose with the recent advances in CT (computed tomography) imaging. Driven by the demands of imaging the beating heart, the scanning time of modern CT scanners enables a dynamic acquisition under movement. As a result, dynamic image-based orthopedics becomes possible. Traditionally, orthopedics relies on anatomical data given by 2D X-ray or 3D CT and MRI imaging. However, previous research has shown that there is a disagreement in quantitative diagnosis results between the traditional and the 3D imaging techniques due to the failure to capture the dynamic nature of joints movement [43]. Accordingly, the benefits of fast modern CT acquisitions have resulted in a novel trend in this area [29, 36], where dynamic scans are acquired in order to understand the complex kinematics, which influence proper joint movement.

There are three main challenges that arise from 4D CT imaging-based orthopedics. The first challenge is the quantification of complex joint movements based on dynamic CT data. While inspecting an animation of the dynamic data might help the medical doctor to get a first impression about underlying conditions, quantification is necessary to support a proper categorization. Since dynamic CT scans contain a vast amount of information, manual calculation of kinematic parameters is a time-consuming process and can lead to inconsistent results. The second challenge lies in the comparative analysis of joint movement patterns. When detected conditions require a surgery intervention, a follow up scan is often performed to measure the success of the operation. However, measuring surgical success requires a comparison of the status before and after the intervention, which makes a comparative analysis necessary. Finally, as medical reporting is required in all medical disciplines, sufficient techniques are required to be able to report on detected conditions.

In the analysis of patello-femoral instability issues, the Skyline or Merchant view captured at 30 to 45 degrees of the knee flexion or 3D CT is commonly used (see Figure 1(a), and 1(b)) [5, 13, 29]. However, these techniques have shown not to adequately reveal the anomaly due to the limitation of capturing the instability of the knee at full extension [14]. With 4D CT, it becomes possible to obtain a 3D visualization of the patella's tracking in the femoral groove during a functional active flexion and extension movement with normal muscular force. As illustrated in Figure 1(c) and 1(d), the ability to obtain information at full extension with 4D CT helps to reveal the anomaly. Furthermore, dynamic CT scans make it also possible to demonstrate the effect of surgical intervention and

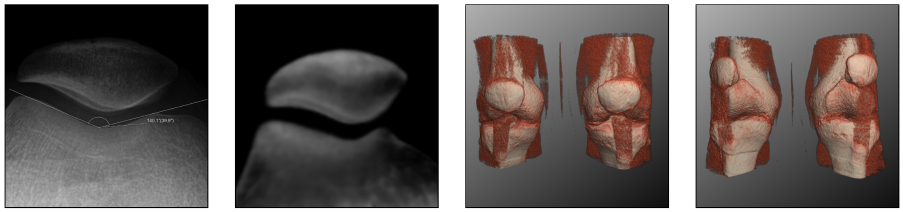

(a) Skyline view (b) Rendering of 3D CT (c) Rendering of a knee at active flexion (d) Rendering of a knee at full extension

Figure 1: 2D and 3D views of a knee joint. While the conventionally used Skyline view captured at 30 to 45 degrees of knee flexion looks normal based on X-ray (a) as well as 3D CT (b), only the joint movement pattern imaged through 4D CT ((c), (d)) reveals the patellar dislocation issue at the full extension.

optimize the surgical technique [5]. The fact that there are more than a hundred of surgical techniques described indicates that no present method is perfect.

To meet the challenges in 4D CT image-based orthopedics, we propose novel visualization metaphors, which enable quantification, comparison, and reporting of joint movements as imaged through time-varying CT data. The proposed metaphors have been developed in close collaboration with medical experts who wish to investigate patello-femoral instabilities with time-varying CT acquisitions. In past years, research has been conducted on the visualization of angular relations. Gait analysis, which is a study of locomotion, can be considered as the origin of kinematic analysis [44]. The central question in this area is the understanding of angle correlations. The angle-angle plot, in which each axis represents a kinematic or kinetic signal, is commonly used to convey angular information. By plotting one signal against the others, an angle-angle plot illustrates the coordinated motion of the two segments or joints. Manal et al. used an advanced color-coding scheme to incorporate additional parameters into the standard angle-angle plot [27]. Later, the authors proposed the use of an additional dimension within the plot so that additional parameters can be visualized [26]. Côté et al. presented 2D projected stick figures to show the kinematic results of continuous hammering performed by different patient groups [10]. While the proposed approach was sufficient when looking at joint height, it failed to reveal the kinematic relationships. Keefe et al. proposed a visualization system based on multiple views to show relationship within sequential kinematic data [19]. Krekel et al. focused on the visualization of the relationships between multiple connected joints by combining interactive filtering with visualization [22]. The approach probably most relevant to our research is that of Krekel et al. [21], in which a technique for visualizing the range of motion of the shoulder joint is presented.

In addition, we propose a GPU-based enhanced FOI identification and tracking in the time domain based on the scale-invariant feature transform (SIFT) algorithm. For instance, the FOIs selected by users are tracked automatically over scans in dynamic CT data and thus, serve as a foundation for quantitative measurement of kinematic parameters. The SIFT algorithm [24, 25] is a widely used technique in the field of computer vision to identify and match features between images. In the SIFT technique, stable features are detected through a scale-space analysis approach. Then, for each detected feature, descriptors are constructed in such a way that they are invariant to rotation, and translation. The constructed descriptors serve as the foundation for matching features between 2D images. While the technique was initially proposed to handle 2D images, the underlying mathematical foundation can be extended to handle n-dimensional data sets [8, 38]. As a result, SIFT has been successfully applied into different application cases involving salient feature localization and matching such as motion tracking [1, 33, 38], group- related studies [42], volumetric ultrasound panoramas [31], and complex object recognition [16, 17]. Recently, SIFT has been compared to other feature detection algorithms and the result shows that SIFT achieves a balanced result between stability and performance [45]. It is worth noting that while the investigation of patello-femoral instability has driven our research, the presented visualization techniques are in fact generalizable and thus can be transferred to other application cases, where complex joint movements are of interest (see Section 6.2).

While other research has been conducted on the visualization of complex joints [22, 35], to our knowledge, the work in this paper is the first to tackle time-varying CT data in order to support the analysis of joint movement patterns. Our visualization approach differs from previous work in the way we handle and derive kinematic information from the input data. For instance, previous research focuses on using markers to track the kinematic behaviors of joints, we focus on extracting kinematic information directly from time-varying volumetric data sets. This enables a new and novel visual interpretation, as the analysis takes arbitrary feature points inside joints into account. Furthermore, patient instrumentation with markers is avoided. To support a better understanding of the acquired data sets and the contained joint movement patterns, we make three major contributions:

- Visualization metaphors for the quantitative assessment and comparison of joint movement patterns.
- Component separation and visualization to enable medical reporting of joint movement patterns.
- Interactive visual inspection of joint movement data based on an enhanced GPU-based feature identification and tracking technique based on the SIFT algorithm.

2. Medical Background

The patella (knee-cap) is a bone that is incorporated into the tendon of the quadriceps muscles of the thigh and moves within a groove at the lower end of the femur (thigh bone). When the knee bends, the patella engages the groove and is fixed to the center of the groove by muscle forces. On the other hand, the patella moves to the upper more shallow end of the groove when the knee is straightened. As a result, the patella will be more loose, and may move somewhat more lateral (to the outside) [37]. The medial patello-femoral ligament (MPFL) is the primary medial restraining structure against lateralization of the patella when the knee is straight or mildly flexed, and contributes up to 80% of the medial restraining forces to the patella [12].

A dislocation of the patella occurs when the patella comes completely out of its groove, gets fixed to the outside of the knee joint, and this causes significant pain. It commonly happens to young and physically active people, often during sporting activities. The annual incidence of primary patellar dislocations has been estimated to 43 per 100000 in children under the age of 15 [32]. The first dislocation usually occurs as a significant injury with the knee in near full extension, but the patella may dislocate much more easily thereafter. Recurrent patellar dislocations eventuate in 15-45% of primary dislocation cases [18] and can cause significant problems, not only prevent sport activity, but also be a hindrance in daily activity.

The primary treatment is bracing as well as physiotherapy to strengthen the stabilizing muscles [2], especially the inner part of the quadriceps muscle (vastus medialis). By strengthening this muscle, it has been hypothesized that the patella will track more centrally in the groove, avoiding a more lateral position that may increase the likelihood of recurrent dislocation and instability symptoms.

In patients who have repeated dislocations, there are more than hundred surgical options described [5]. It is possible to restore the normal anatomy by repairing the torn ligaments on the inner aspect of the knee, to deepen the groove, or to realign the patellar tendon to stabilize the patella in a more medial (inner) position [37]. In the last decade, it has been increasingly popular to reconstruct the MPFL, often as an isolated procedure [9].

The lack of accurate follow-up methods to assess the movement of the patellar in relation to the groove after rehabilitation or surgical intervention has led to the multitude of operations. Ordinary radiographic methods are inadequate for the assessment of patello-femoral malalignment. The most commonly used technique for visualization of the patello-femoral joint requires 30 to 45 degrees of knee flexion (see Figure 1(a)) [5, 11, 41]. It is a static examination and the images are not obtained near full extension where the groove is most shallow and the patella is more unstable. Conventional CT-scans and MRI can get images with a straight knee, but they are static and will not display patellar tracking under functional movements (Bull, Katchburian 2002). With the use of 4D CT, it becomes possible to get a 3D visualization of the patella's tracking in the femoral groove during a functional active flexion and extension movement with normal muscular forces. However, it is difficult to describe 3D motion in a distinct way. Fixed body axes in either the patella or femur can give confusing results [5]. Thus, there is a great need for quantitative analysis of joint movements through apparent visualization methods to give a better understanding and also to get quantifiable results.

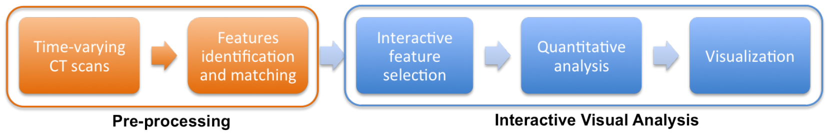

Figure 2: In the pre-processing stage, features in a dynamic CT data set are extracted and matched between scans. In the second stage, user can select FOIs and have these FOIs tracked in the time domain. Depending on the application in mind, different quantitative measurements can be performed and visualized for assessment.

3. Method

Figure 2 presents the workflow of the proposed approach. In order to support the quantitative visual analysis of the knee movement patterns, the dynamic CT scan is pre-processed. Particularly, features are extracted and matched between scans to serve as the foundation for the interactive visual analysis stage. In the second stage, users can interactively select FOIs and the system automatically tracks these features between scans in the input dynamic CT data. Depending on the application in mind, different quantitative measurements of kinematic parameters based on the selected features are performed. The results are then visualized through the proposed visual metaphors (see Section 4) to support quantitative and comparative analysis of the underlying kinematic information.

3.1. Enhanced GPU-based feature identification and tracking

While our work is based on extensions of the SIFT algorithm to handle 3D volumetric data [38, 8], we exploit the parallel nature and computing power of the GPU to achieve interactivity. Moreover, we propose a novel descriptor construction technique that helps to improve the accuracy in the feature matching and tracking process. The algorithm is performed in three successive stages: *feature location detection*, *feature descriptor construction*, and *feature matching*.

3.1.1. ***Feature location detection***

In the first stage, stable features in the input image are identified through a scale-based analysis approach. First, the volumetric input data, $I(x, y, z)$, is convoluted with variable-scale Gaussian functions, $G(x, y, z, k\sigma)$, to generate a scale space, $L(x, y, z, k\sigma)$, as follows:

$$L(x, y, z) = G(x, y, z, k\sigma) * I(x, y, z) \tag{1}$$

where k is a constant multiplicative factor for separating scales in the scale-space. The local extrema of the difference-of-Gaussian functions, $D(x, y, z, k^i\sigma)$, applied to this scale space are considered to be potential local features in the original volumetric data:

$$D(x, y, z, k^i\sigma) = L(x, y, z, k^{i+1}\sigma) - L(x, y, z, k^i\sigma) \tag{2}$$

Lindeberg and colleagues could show that these local extrema are a close approximation to the scale normalized Laplacian-of- Gaussian [23], $\sigma^2\nabla^2G$, which are the most stable features in the input image [30]. By applying a thresholding scheme based on the principle curvature analysis to filter out the blob-like and edge-like features, which are usually of no interest, the stability of the detected feature locations can be further improved [1].

The construction of the scale-space representation is a computation demanding process. Fortunately, the calculation at each voxel is independent of the calculation at others. Therefore, it is natural to make use of the parallel nature of the GPU to enhance the performance. For instance, the convolution of the input volumetric data using separable Gaussian kernels helps to dramatically improve the performance.

3.1.2. ***Feature descriptor construction***

The aim of the second stage is to construct a unique descriptor to represent the detected feature location in such a way that is most invariant with respect to rotation, scaling, and translation. The construction of such a descriptor is based on the gradient orientations in the neighborhood of the detected feature locations and presented as a histogram of gradient orientations. In 3D, a gradient orientation comprises three components: azimuth, elevation, and tilt angle. While the elevation and azimuth components can be derived directly from the gradient itself, the tilt angle can only be derived through a more complex analysis of the neighborhood [1]. Consequently, a 2D histogram is required to capture the distribution of the azimuth and elevation angles when handling 3D images.

In the first step of constructing a descriptor, it is crucial to identify the dominant gradient orientation, which is the maximum peak in the histogram of gradient orientations, in the neighborhood of a detected feature. The rotation invariant property of the descriptor is achieved by re-orienting the other gradient orientations in the neighborhood to the identified dominant gradient orientation before generating the final descriptor [25]. In addition, to avoid disruptive changes of gradient orientations in the neighborhood around a detected feature location and to further improve the uniqueness of the constructed descriptors, gradient orientations are divided into ranges of 45 degrees, and the neighborhood around each detected feature location is divided into sub-regions [1, 25]. For example, the commonly used neighborhood size of 16x16x16 is divided into 64 sub-regions of 4x4x4. Thus, the final descriptor is a concatenation of histograms of gradient orientation corresponding to each sub-region. While the resulting descriptor is a unique representation of the detected feature, discarding the other gradient orientations of lower magnitude can have a negative impact on the feature identification stage. By creating additional descriptors based on smaller peaks, which are of 80% the maximum peak in the initial histogram of gradient orientations, the accuracy in the feature matching process can be vastly improved [25].

Previous research has shown that the size of the neighborhood can have a large impact on the uniqueness of the constructed descriptors, which affects the accuracy of the feature matching process between images [1, 33]. This is due to the fact that the size of the neighborhood is a global setting and is dependent on the input data. While a large size neighborhood (e.g., greater than 16x16x16 voxels) might fail to capture the local characteristic of the detected feature, a small size neighborhood (e.g., less than or equal 8x8x8 voxels) might put too much emphasis on the local property characteristic of the detected feature. To overcome this limitation, we propose a novel descriptor construction approach called *ring descriptor*. In our approach, the neighborhood is divided into non-overlapping sub-regions centered at the detected feature location. For each non-overlapping sub-region, the dominant gradient orientation is identified. This allows us to capture not only the local characteristic of the detected features but also reduce the impact of the neighborhood size setting on the uniqueness of the final descriptor. To achieve rotation invariant property, gradient orientations in the neighborhood are then re-oriented to the dominant gradient orientations of each sub-region before the construction of the histogram of gradient orientation. Our experimental findings have shown that not only the total number of descriptors is comparable to previous approaches, but also the uniqueness of the descriptors is increased. Consequently, the proposed descriptor construction technique helps to improve the accuracy of the feature matching process without scarifying the performance, which will be presented in detail in Subsection 6.1.

Another advantage of the proposed technique is the ability to introduce a weighting factor into the feature descriptor construction process. For instance, depending on the input data, the local property of the detected feature can be emphasized or de-emphasized through a weighting factor for the dominant gradient orientation of the non-overlapping rings. As a result, the size of the neighborhood has less influence on the result, which makes the proposed approach more flexible in handling different type of dynamic volumetric data.

One of the challenges for the realization of the proposed approach using the graphics hardware is the limitation of the memory architecture of the GPU. For instance, a large neighborhood setting can lead to a large histogram that cannot be fitted into the local/share memory on the GPU to exploit the highest performance as possible. To overcome this limitation, a multi-pass approach can be used [39]. In our approach, we have different OpenCL kernels that are optimized for different histogram size and a generic kernel for handling large size histogram. The system then automatically switches between optimized versions to achieve the highest performance.

It is worth mentioning that a smoothing operator applied to the constructed histogram of gradient orientations is required to reduce the impact of disruptive changes of gradient orientations [25] in standard implementation of SIFT. However, the type and the bounds of the smoothing operator are abstracted from the original input data. As a result, it is difficult to identify a good smoothing operator to improve the quality of the constructed descriptor. In the proposed technique, by moving the computing from CPU to GPU, we do not only exploit the parallel computing power of the GPU but also implicitly achieve the interpolation supported by the hardware. Particularly, the GPU hardware enables us to achieve a bi-linear interpolation by default. Moreover, instead of re-orienting gradient orientations in the neighborhood around a detected feature location, the whole neighborhood is re-oriented to the dominant orientation and gradient orientations are updated accordingly. This allows us to minimize the effect of different interpolation scheme applied to a constructed histogram of gradient orientations as the interpolation in our approach is directly based on the underlying information from the input data.

3.1.3. ***Feature matching***

Once the features descriptors have been constructed for two data sets to be compared, they can be used to identify matching features using different techniques such as RANSAC [15], Best-Bin-First (BBF) [3]. Since a descriptor is basically a concatenation of histogram of gradient orientations, the Euclidean distance between descriptors is a good indicator for a high probability match:

$$d(p, q) = \sqrt{\sum_{i=1}^{N} (p_i - q_i)^2} \tag{3}$$

Here, p and q are two descriptors, p_i and q_i are the i-th elements of these descriptors, and N is the size of the descriptors. To find the matching features in the two data sets, I_1 and I_2, the Euclidean distances from each descriptor in I_1 to all descriptors in I_2 are computed. The minimum distance value is an indicator of a high probability match. The finding of the minimum distance is a reduction problem. Due to the size of each descriptor, a GPU-based approach does not improve the performance. As a result, we present a hybrid approach to the problem of feature matching. The computation of the Euclidean distance between one descriptor in the first input image, I_1, and all descriptors in the second image, I_2, are performed in parallel using the GPU. The result is then passed to the CPU implementation to identify the minimum distance that serves as indication of a high probability match.

3.2. Kinematic parameters measurement

There have been various researches focusing on the methods used to describe patello-femoral joint motion in past years. The results can be classified into two groups: those that describe motion of the patella relative to the femoral groove and those that describe the motion of the patella relative to a fixed-body axis [5]. The former are primarily imaging studies, in which CT and MRI have been used to investigate the patellar motion during dynamic knee joint movement [4, 34, 40]. One significant drawback of previous results is the inability to describe the patellar motion in three-dimensional space.

The congruence and tilt angles between the patellar and the femoral groove are two commonly used kinematic parameters in quantitative analysis of the patello-femoral issue. As the congruence and tilt angles reflect the relation between the patellar and the femoral groove, we propose a geometry setup, in which the patellar and the clip plane cut through its widest part serve as the reference, for quantitative kinematic measurement (see Figure 3). The congruence angle is then defined by the angle between the bisected femoral trochlea (dashed

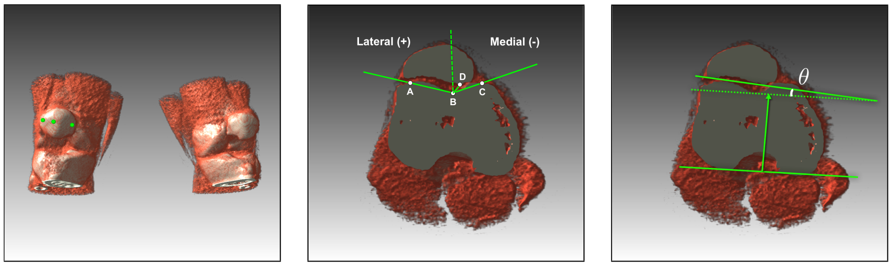

(a) Knee overlain with a FOI (green) (b) Congruence angle measurement (c) Tilt angle measurement

Figure 3: Congruence and tilt angle measurement. (a) is the visualization of the knee overlain with a FOI (green), which marks the widest part of the on the left knee. (b) and (c) are the illustrations of the congruence and tilt angle measurement through a clip plane setup.

line in Figure 3(b)) and the vector connecting the apex of sulcus angle, ABC, to the lowest point of the articular ridge of the patella (BD in Figure 3(b)). By using the same geometry setup, the tilt angle, θ, is defined as the angle subtended by a line joining the lateral edge and the lowest point of the articular ridge of the patella and the posterior condylar line as illustrated in Figure 3(c).

Besides the ability to describe the patellar motion in three-dimensional space, the combination of the proposed kinematic parameters measurement approach and the feature identification and tracking allows us to have a semi- automatic measurement of kinematic parameters. The manually selected FOIs (see Figure 4(a)) are automatically tracked across scans in a dynamic data set. As a result, the resulting clip plane setups can be achieved not only automatically but also consistently.

It is worth pointing out that when the patella moves out of the femoral groove, there is no intersection between the clip plane and the femoral groove, thus the congruence angle cannot be calculated. Consequently, the proposed approach reflects the fact that there is no congruence between the patella and the femoral groove, which the previous research results failed to capture and present.

In addition to the measurement of the congruence and tilt angle, we propose the measurement of the distance, d_G, from the lowest point of the articular ridge of the patella, R, to the femoral groove to convey the translation of the patella in relation to the femoral groove as follows

$$d_G = \min_{1 \leq i \leq N} d(R, p_i) \tag{4}$$

where N is the number of point on the femoral groove, and d is the Euclidean distance function. In this approach, the femoral groove is approximated by a set of discrete point in order to reduce the computation demand. The presented feature tracking technique allows us to track the identified points, which approximate the femoral groove, in the time domain to facilitate the calculation and reduce the time-consuming process of manually select features through out all the scans in a dynamic data set. By applying the same approach, the distance

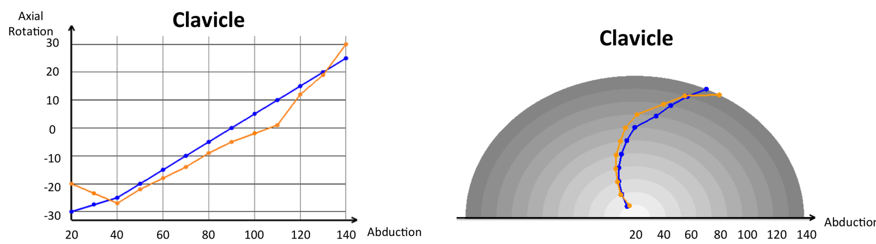

(a) Angle-angle plot

(b) Radial angle plot

Figure 4: The relations between the abduction angle and the axial rotation of two subjects. The standard angle-angle plot allows quantification of the relation but makes mental registration with the spatial context difficult (a). The proposed radial angle plot represents the same data in a joint centered way, while at the same time exaggerating the differences for critical abduction angles (b).

between the drill holes on the patella and the drill hole on the femoral can also be calculated. The quantitative results enable doctors to assess the success of the surgical intervention in comparison to the pre-surgical intervention as well as the effect after the surgical intervention.

4. Comparative Visualization

4.1. Radial angle plot

The angle-angle plot is one of the most commonly used visual metaphor for depicting kinematic parameters [27]. In a traditional set up, each axis of the plot represents a kinematic parameter, whereby the plot reveals the relation of the individual parameters to each other. Figure 4(a) shows an example of the angle-angle plot depicting the relations between the abduction angle and the axial rotation of two subjects. Although the angle-angle plots help to reveal the relations between the two kinematic parameters, its representation does not reflect the visual mapping of the presented angular values within the context of the joint. As a consequence, the interpretation as well as the mental linking of the plot to the actual movement patterns requires a lot of experience and time. This becomes especially apparent when observing the comparative qualities of the angle-angle plot. When comparing the plotted data for Patient 1 (*orange*) and Patient 2 (*blue*), it becomes clear that the movement of Patient 1 includes a lower degree of axial rotation for abduction levels 40 to 130. However, as the spatial reference of the joint is missing, the rotation difference with respect to the joint is not immediately visible.

To address these shortcomings, we present *radial angle plots* as a joint-centered visualization metaphor to depict kinematic parameter relations. The radial angle plots have been designed in such a way that they can be easily applied to various joint types. Instead of using linear mappings for the x and the y-axis as illustrated in Figure 4(a), we combine linear and polar mappings of the angular values. While the x-axis is the linear representation of one kinematic parameter, the y-axis is converted into a polar representation as shown in Figure 4(b). This enables the visual mapping of the plotted values to the actual angular changes, as given within the frame of reference of the joint under investigation. The concentric layout of the angular relations between kinematic parameters provides an implicit exaggeration of the most interesting kinematic parameter range, i. e., an angle representing full abduction or flexion. These extreme angles are the most problematic when dealing with joint issues, even small changes need to be considered and should thus be emphasized by the used visualization metaphor.

Figure 4 compares the traditional angle-angle plot to the proposed radial angle plot. In Figure 4(b), the x-axis represents the abduction angle while the axial rotations are placed on the corresponding shaded concentric half-circle (from -90 degrees to $+90$ degrees, from left to right). The gray scale gradient has been chosen to allow an intuitive quantification of the polar angle coordinates, as well as an emphasis of the joint center, which is located in the middle at 0 degrees. While the angle-angle plot also depicts the relations between the two kinematic parameters for both patients, the radial angle plot reflects the actual angular changes directly through its visual mapping.

When dealing with the patello-femoral analysis, which is addressed in Section 5, an additional benefit of radial angle plots is the fact, that they can be directly co-registered with the 2D Skyline view representation. As illustrated in Figure 5, the concentric layout and the polar representation of the congruence values not only enables us to emphasize the difference between pre- and post-operation result at extreme position (53 degrees flexion) but also implicitly co-registers the rotation to of the kneecap to the femoral groove (center of the radial angle plot). Moreover, the radial angle plot also reflects the medial and lateral patellar angles corresponding to the negative and positive halves of the rendering. It is worth pointing out that in the design of the radial angle plot, the range of the angular value can be normalized accordingly to emphasize the changes.

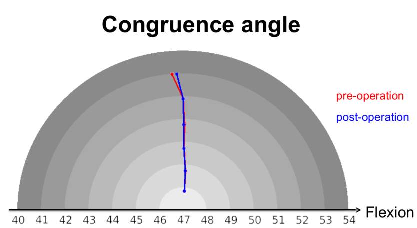

Figure 5: A radial angle plot of the congruence angles from pre-operation (red) and post-operation (blue).

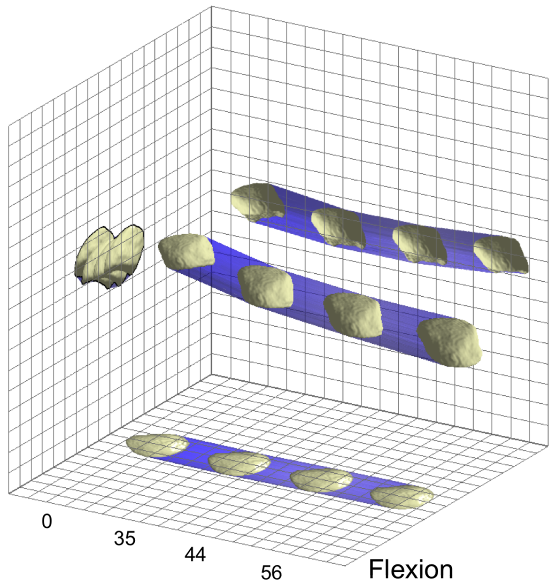

Figure 6: Visualization of the proposed time-angle profile metaphor. The extracted movement pattern of the patellar over time is rendered at the center of the image. Kinematic parameters are incorporated through projection technique onto the bottom, side, and back plane.

4.2. Time-angle profile

Although the 3D visualization of a full scan in a time-varying data set can provide both the visual context and the detail information to support visual analysis, there is a large amount of data presented to the user, especially in the case of 4D CT. In addition, the occlusions in the 3D visualization of volumetric data can change drastically in the time domain, and affect the visual access to areas of interest. Consequently, this can cause distractions when a user changes from one time frame to another. As the kinematic analysis process usually focuses on a defined feature and derive its movement patterns over time, an abstract visualization focusing on the feature and its kinematic characteristic can help to improve the visual analysis process. We propose an abstract visualization of a defined feature in the time domain called *time-angle profiles*. The proposed visual metaphor is designed in such a way that it helps to filter out unnecessary information while maintaining the kinematic parameters of the feature under investigation. At the same time, it captures the whole movement within a single picture and thus supports medical reporting and pattern comparison.

To generate this representation, the feature must be identified in all time frames before all instances are combined into a single visualization. In a standard approach, the extraction of the feature under investigation in all scans of a dynamic data set is very time-consuming. Fortunately, the proposed feature identification and tracking technique allows us to derive affine transformations of the feature across all scans in the dynamic data. As a result, a single extraction of the feature is enough for the generation of the proposed visual representation. The combination of all instances of the feature in all time frames is then visualized through a 3D sweep structure. This sweep representation provides an overview of the whole kinematic changes in the time domain. However, it does not facilitate visual assessment of kinematic parameters due to the fact that a complex movement pattern is usually a combination of different components such as rotations, translations, and tilting. Inspired by the magic mirror metaphor introduced by König et al. [20], we exploit the use of projection techniques to decompose the movement patterns for the extracted features. By projecting the whole movement pattern onto a multi-planar plane geometry, we can reveal the underlying components of the kinetic parameters. For instance, a projection from the top view can reflect the rotation, and a projection from the side view can shows the translation over time. In addition, the semi-transparent sweep structure is color coded to depict the various degrees of kinematic parameter changes.

Figure 6 illustrates the proposed visual metaphor applied to the visualization of the movement pattern of the patellar. At the center of the image is the extracted movement pattern of the patellar over time. The transition from a lighter to a darker color depicts the degree of kinematic parameter changes. For instance, as the patellar rotates, tilts and translates more at the extreme position in comparison to the initial relaxed one, the color goes from a dark to a light shade of blue. By projecting the movement pattern using different viewing angles, the proposed visualization approach can achieve the decomposition of the complex kinematic characteristics. The orthographic projection of the trajectory onto the side plane reveals the shifting of the patellar out of its groove. The projection onto the bottom plane reflects the changes in congruence angles, while the projection onto the back plane shows the degree of tilting. Although the proposed technique does not provide the contextual information by focusing only on the movement pattern, it can be used as an adjunct to the 3D visualization of the time-varying data in a multiple linked view setup. As a result, contextual information and an overview of the kinematic changes over time can be visualized in an integrated manner.

5. Results and Discussion

We applied to proposed approach to two real clinical data sets to verify the ability to facilitate quantitative analysis of the patellar movements. Two subjects were examined for this study. The first subject is a 19 years old female, patient A, with bilateral pronounced instability problems since she was 13 years old without any significant injury. The left and right side of patient A were operated in 2011 and 2012 respectively. The left side has been stable since the operations and is now asymptomatic. However, patient A had an injury on the right side after the operation. The situation makes it hard to assess the reconstructed tendon with CT scan on the right side on which patient A still has some instability symptoms. As a result, a re-rupture or an elongation of the

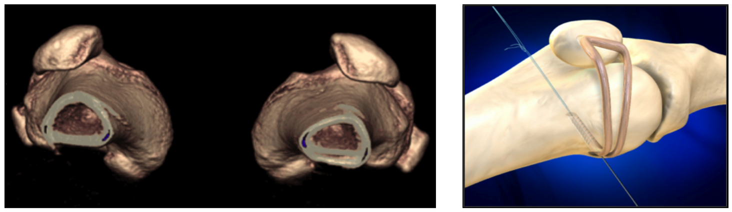

(a) (b)

Figure 7: Visualization of straight knees before the operation (a), and the reconstruction of MPFL with a gracilis tendon (b) (permitted by Storz).

reconstruction are under suspicion. The second subject is a 23 years old male, patient B, with distinct problems after an injury on the left side. In addition, patient B also has minor instability problems on the right side. Patient B had an operation on the left side in 2013. The operation was successful and patient B has a stable knee three month after the operation.

Figure 7(a) illustrates an overview of the patello-femoral issue in both cases, in which the kneecaps are far out and tilted on the lateral side. In both cases, the operations were performed with a reconstruction of the MPFL with a gracilis tendon (see Figure 7(b)). First, two drill holes on the kneecap and another one on the femur were created. Then, the tendon is passed through the drill holes on the kneecap, both free ends are then passed into the drill hole on the femur, tightened with the use of sutures and then fixed with a resorbable screw in the femur.

About a month before the operation, a dynamic CT scan is performed. The patient is supine with both legs resting on a radiolucent knee-support as illustrated in Figure 8. The maximal knee angle is about 40-50 degrees when the heels are touching the bed as shown in Figure 8(a). The patient performs bilateral active knee extensions until full extension (see Figure 8(b)), referenced as 0 degree, and then flexions.

The acquired dynamic CT scans were pre-processed using the GPU-based enhanced FOI identification and tracking approach proposed in Subsection 3.1. In the quantitative visual analysis stage, the domain experts interactively se-

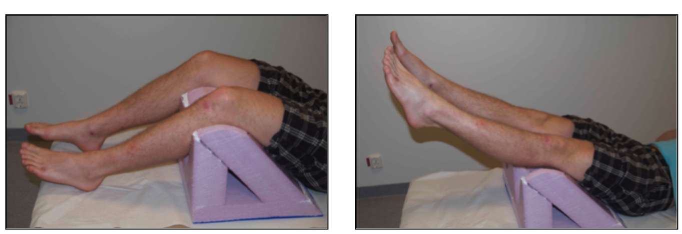

(a) (b)

Figure 8: Flexion (a) and extension (b) of the knees resting on the radiolucent knee support.

lect FOIs (see Figure 3(a)) in one time frame and have these FOIs tracked automatically through the whole dynamic CT scan. Consequently, kinematic parameters were calculated in an automatic manner. The results were then presented through the proposed visualization metaphors to convey the underlying kinematic parameters of interest.

Figure 9 presents the quantitative measurements of the distance from the lowest point of the articular ridge of the patella to the femoral groove. Patient A had subluxations of both kneecaps when straightening the knees before the operation. On the postoperatively asymptomatic left side, the distance to the groove has decreased from about 60 mm to 25 mm with straight knees. On the right side, patient A still has some instability symptoms; however, it is less than before the operation, the distance to the groove has decreased from about 53 mm to 28 mm. The result of the facilitated the measurement of the distance from the two drill holes on the kneecap to the one on the femur for patient A is presented in Figure 10. The measurement shows that the distances are stable between the 3 month post-operation and 12 month post-operation.

Figure 11 shows the result of tilt angle measurements using the technique proposed in Subsection 3.2. The proposed radial angle plot present not only the movement patterns of the kneecap but also present them with respect to the reference frame, which is the femoral groove. Figure 11(a) shows that the tilting pattern of the left and the right kneecap are similar. Due to the injury happened after the operation in 2012, patient A still has instability issue on the right side. Although the tilt angles are similar between the left and right side at full extension, the patterns are different when the functional movement comes to 45 degrees flexion, which is emphasized through the radial angle plot in Figure 11(b).

The movement patterns of the left kneecap of patient B are depicted in Figure 12. The decomposition of the complex kinematic properties are done through the projection technique. Particularly, the projection onto the side presents the shifting of the kneecap out of its groove. The projection onto the bottom plane reflect the congruence angle changes, and the projection onto the back plane conveys the tiltings of the kneecap with respect to the femoral groove. From Figure 12(a) and Figure 12(b), it can be seen that the kneecap shifts out of

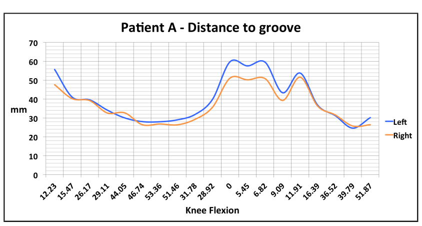

(a)

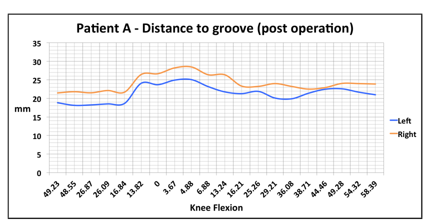

(b)

Figure 9: Quantitative measurement of the distance from the lowest point on the articulate ridge to the femoral groove before operation (a), and post operation (b) from patient A.

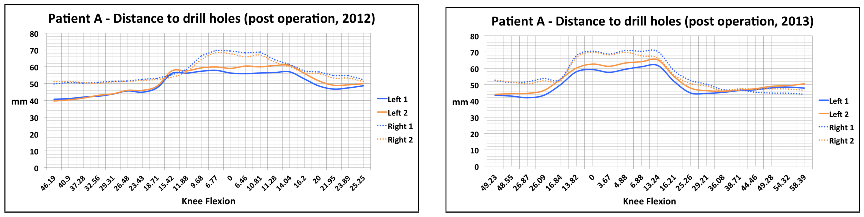

(a) (b)

Figure 10: Distance between the drill holes on the kneecap to the drill hole on the femur three month after the operation (a), and one year after the operation (b) for patient A. The measurements showed that the distances are stable between 3- and 12 month postoperatively.

the femoral groove less after operation. In addition, the changes of tilt angles as well as the congruence angles are also less than before. In addition to the detail rendering of the transformation of the kneecap, the color-coding scheme also quickly provides the information about the kinematic changes. For instance, the color transition from dark to light between the 48 degrees and 35 degrees flexions in the rendering on the back plane indicates that the tilt angle reduces rapidly. On the other hand, the small color transition from 44 to 46 degrees flexion in the rendering on the bottom plane indicates that the congruence angle stays almost unchanged. This reflects the fact that the operation on the left side of patient B was successful.

According to the feedback from domain experts, the quantitative measurements facilitated by our proposed approach support the suspicion of the doctor about the instability of the right knee of patient A. For instance, patient A had a more pronounced decrease of the groove distance for the asymptomatic left knee postoperatively compared to the right one, but both legs of the ligament reconstruction were unchanged according to the the distances between the drill holes between 3 months and 12 months postoperatively. This indicates that the injury happened after the operation could have elongated the reconstructed ligaments on the right side, but there were no further elongation the rest of the first postoperative year. Moreover, we also receive positive feedback from domain experts about the time-angle profiles. This visual metaphor is very

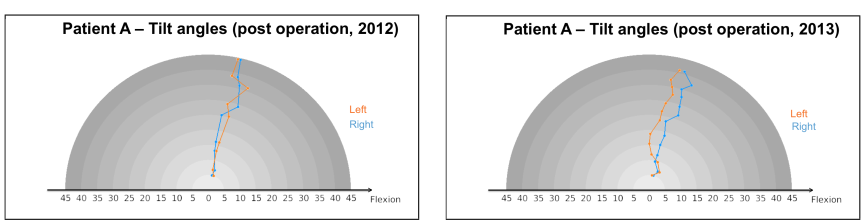

(a) (b)

Figure 11: Quantitative measurement from the proposed approach for the tilt angles of the kneecaps for patient A.

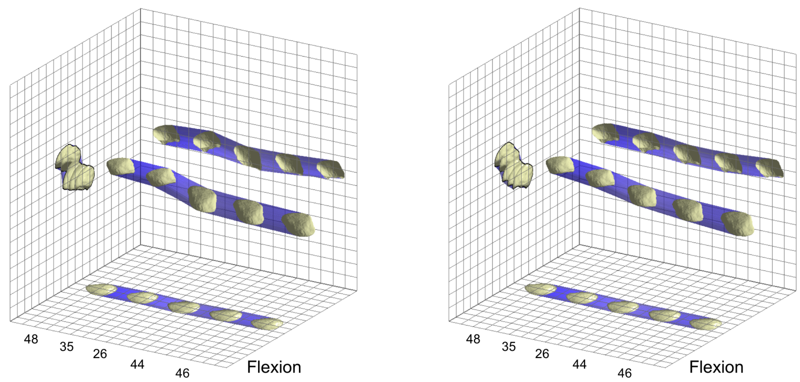

(a) (b)

Figure 12: Visualization of the movement pattern of the left kneecap of patient B using the time-angle profile visual metaphor. (a) and (b) present the measurements of kinematic parameters from pre- and post-operation stage respectively.

useful in providing an overview of the movement pattern of the patellar under investigation. Besides the ability to decompose a complex movement pattern into several kinematic parameters through projection technique, the combination with the facilitated automatic kinematic parameters measurement enables the transition from an overview into a detail quantitative analysis.

6. Verification and Generalization

6.1. Verification

To evaluate the proposed GPU-based enhanced FOIs identification and tracking, we compare our results to the recently published work [33]. The test data set is a 4D CT thorax scan [7, 6]. The data is given by ten equally sampled phases of the respiratory cycle in which the maximum exhale phase and the maximum inhale phase are denoted as $L0$ and $L5$ respectively. The reconstructed volumes have the size of 512x512x128 voxels. The reference landmarks in $L0$ and $L5$ were manually setup by domain experts. While the parameters used in our algorithm were set to match the ones used in [33], our approach makes use of the proposed *ring descriptor* construction technique. In addition, due to the advantage of the GPU-based implementation, we do not apply smooth operator to the histogram to avoid disruptive changes of gradient orientations but instead rotate the neighborhood region to the dominant orientation, which implicitly takes advantage of the bi-linear interpolation on the GPU.

6.1.1. ***Feature location detection***

We have evaluated the matches, whereby we have computed the error as 3D residual distance between identified and matched feature locations at the $L0$ and the $L5$ phase (SIFT $L0$–$L5$). Figure 13 illustrates the visualization of the

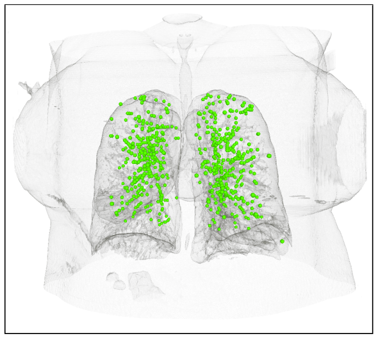

(a)

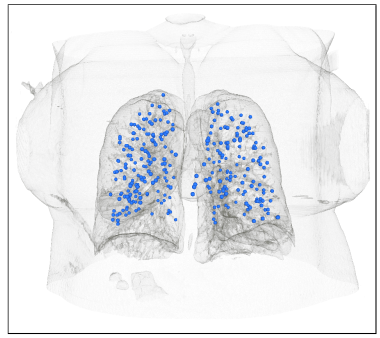

(b)

Figure 13: Visualization of the inhale lung. (a) is the visualization of the lung overlain with the detected feature locations (green) from the GPU-based enhanced FOI identification and tracking algorithm, (b) is the visualization of the inhale lung with the manually input landmarks (blue).

inhale lung overlain with features of interest. While the detected features from the SIFT algorithm are colored in green (Figure 13(a)), the manually input reference landmarks are colored in blue (Figure 13(b)). The Mann-Whitney U test [28] was applied to the error distribution in the identified and tracked features as well as in the reference landmarks. Table 1 shows our results in comparison to the ones reported in [33]. Besides the slightly higher number of matches between the maximum exhale and maximum inhale phase, the proposed approach has shown to improve the accuracy in the descriptor matching process, as we have achieved a lower median, 11.14 compared to 13.23, as well as a lower variability. In addition, the Mann-Whitney test confirms that the distributions of the residual distances in the reference landmarks and in the result of the enhanced SIFT operator are not significantly different (p-value = 0.736), which means that the proposed approach can be used to identify the feature locations.

6.1.2. ***Feature matching***

To measure the impact on the feature matching process, we detect the feature locations in the time-series data and track these features in two different variants. First, we always use the maximum exhale phase, $L0$, as a reference.

Table 1: Number of matches, median and variability of error distributions at maximum exhale, L0, and maximum inhale, L5, phases obtained by the proposed enhanced SIFT compared to results from previous work [33] and the manual reference landmarks. Variability is the difference between the 25th and 75th percentiles.

	#Matches	Median (mm)	Variability (mm)
$L0$–$L5$	300	12.98	18.22
SIFT ($L0$–$L5$)	509	13.23	17.90
Proposed technique ($L0$–$L5$)	525	11.14	12.78

Table 2: Number of preserved feature locations along the breathing cycle from the maximum exhale, $L0$, to the maximum inhale, $L5$, phase.

	SIFT ($L0$–$L5$)	Proposed technique ($L0$–$L5$)
Reference (Phase 0)	117	243
Along breathing cycle	9	264

Second, we move step-by-step along the breathing cycle such that the previous breathing phase is served as the reference for tracking the feature locations in the next breathing phase. For each approach, we computed the number of feature locations between all phases. Table 2 reports the number of detected feature locations which were preserved along the breathing cycle. While tracking along the breathing cycle allows us to achieve a higher number of preserved feature locations and excludes the trailing ones, tracking referred to a reference phase excludes the most stable feature locations over time. The results in Table 2 shows that ours technique allows a more stable feature tracking in dynamic data set.

As reported in Table 1 and Table 2, the proposed enhanced descriptor construction helps to increase the uniqueness of the descriptors at feature locations. Thus, it helps to improve the accuracy of the feature matching process in time-series data. It is also worth noting that by exploiting the power of the GPU implementation, we also achieved a much better performance in time. For instance, the overall time required for descriptors generation for each volume and descriptors matching between volumes is approximately 5.0 minutes. This is ten times faster than the result in [33], which is 50 minutes. As for the interactive visual analysis, the feature descriptors and be pre-computed and thus, the interactivity can be achieved.

6.2. Generalization

Although the data analyzed and visualized in this work has been extracted from the patello-femoral analysis scans, the presented techniques can be extended and applied to different kind of joint movement analysis. As shown in Subsection 6.1, the proposed GPU-based feature identification and tracking can be applied to dynamic CT scans in general. Depending on the application in mind, different criteria for FOIs selection and kinematic parameters calculation can be implemented based on the tracking results.

The time-angle profile visual metaphor was designed in such a way that it can be easily extended through the use of different projecting criteria. By deploying different projection criteria, the time-angle profile visual metaphor can be used for visual analysis of different underlying kinematic parameters. Moreover, these projections can be co-related through a multiple linked-views setup to facilitate both the overview of the whole movement pattern as well as detail decomposition of the kinematic behavior under investigation.

Figure 4 already shows the application of the radial angle plot to visualize the kinematics of a ball joint. The joint-centered nature of the radial angle plot is clearly an advantage, as it allows a quantified interpretation of the rotational angle without hindering the embedding into the spatial context. To incorporate the additional degrees of freedom, either the plot can convey several kinematic properties, or multiple radial angle plots can be combined. As an alternative to these two variants, also parallel coordinate views could be integrated to show the correlation between different angles [22]. Finally, while the current radial angle plot supports a angle domain of $[-90; +90]$, increasing the arc length can be used to represent larger angle domains.

7. Conclusions & Future Work

In this paper, we have presented new visual metaphors for the interpretation kinematic information derived from dynamic CT data sets. In addition, we proposed an enhanced GPU-based feature identification and tracking based on the SIFT algorithm. Besides the performance improvement, thus allows interactive feature identification and tracking, the proposed technique also achieve a higher accuracy in the process of feature matching based on the novel descriptor construction approach. We have applied the introduced techniques to the analysis of the patello-femoral issue. Integrating the presented techniques into the analysis process of 4D CT scans has shown great potential as the quantitative measurement results from the system reflect the real clinical situation of the patients. Moreover, the presented visual metaphor enables medical doctors to have not only a quick overview of the movement pattern of feature under investigation in the dynamic CT scans but also the underlying kinematic information.

In the future, we would like to acquire 4D CT data of the shoulder joint and verify the application of the proposed visualizations. Furthermore, we plan to use our approach to derive a normal collective, which would allow us to automatically emphasize abnormal movement patterns. When dealing with a system of multiple joints for each patient, we would also like to combine multiple radial angle plots into a single view. Finally, we would like to investigate how time-angle profiles could be extended to support an embedding of several individuals.

References

[1] Allaire, S., Kim, J.J., Breen, S.L., Jaffray, D.A., Pekar, V., 2008. Full orientation invariance and improved feature selectivity of 3D SIFT with application to medical image analysis. IEEE Computer Society Conference on Computer Vision and Pattern Recognition Workshops , 1–8.

[2] Beasley, L.S., Vidal, A.F., 2004. Traumatic patellar dislocation in children and adolescents: treatment update and literature review. Current Opinion in Pediatrics 16, 29.

[3] Beis, J.S., Lowe, D.G., 1997. Shape indexing using approximate nearest-neighbour search in high-dimensional spaces. Proceedings of the 1997 Con-

ference on Computer Vision and Pattern Recognition (CVPR '97) , 1000–1006.

[4] Brossmann, J., Muhle, C., Schröder, C., Melchert, U.H., Büll, C.C., Spielmann, R.P., Heller, M., 1993. Patellar tracking patterns during active and passive knee extension: evaluation with motion-triggered cine MR imaging. Radiotherapy and Oncology 187, 205–212.

[5] Bull, A.M.J., Katchburian, M.V., Shih, Y.F., Amis, A.A., 2002. Standardisation of the description of patellofemoral motion and comparison between different techniques. Knee Surgery, Sports Traumatology, Arthroscopy 10, 184–193. doi:10.1007/s00167-001-0276-5.

[6] Castillo, E, Castillo, R., Zhang, Y., Guerrero, T., 2009. Compressible image registration for thoracic computed tomography images. Journal of Medical and Biological Engineering 29, 222–233.

[7] Castillo, R, Castillo, E., Guerra, R., Johnson, V.E., McPhail, T., Garg, A.K., Guerrero, T., 2009. A framework for evaluation of deformable image registration spatial accuracy using large landmark point sets. Physics in Medicine and Biology 54, 1849–1870.

[8] Cheung, W., Hamarneh, G., 2007. n-SIFT: n-Dimensional Scale Invariant Feature Transform. IEEE Transactions on Image Processing 18, 2012–2021.

[9] Christiansen, S.E., Jacobsen, B.W., Lund, B., Lind, M., 2008. Reconstruction of the Medial Patellofemoral Ligament With Gracilis Tendon Autograft in Transverse Patellar Drill Holes. Arthroscopy: The Journal of Arthroscopic & Related Surgery 24, 82–87. doi:10.1016/j.arthro.2007.08.005.

[10] Côté, J.N., Raymond, D., Mathieu, P.A., Feldman, A.G., Levin, M.F., 2005. Differences in multi-joint kinematic patterns of repetitive hammering in healthy, fatigued and shoulder-injured individuals. Clinical Biomechanics 20, 581–590.

[11] Davis, D.K., Fithian, D.C., 2002. Techniques of Medial Retinacular Repair and Reconstruction. Clinical Orthopaedics and Related Research 402, 38–52.

[12] Desio, S.M., Burks, R.T., Bachus, K.N., 1998. Soft Tissue Restraints to Lateral Patellar Translation in the Human Knee. The American journal of sports medicine 26, 59–65.

[13] Elias, D.A., White, L.M., 2004. Imaging of patellofemoral disorders. Clinical Radiology 59, 543–557. doi:10.1016/j.crad.2004.01.004.

[14] Endo, Y., Stein, B.E.S., Potter, H.G., 2011. Radiologic Assessment of Patellofemoral Pain in the Athlete. Sports Health: A Multidisciplinary Approach 3, 195–210.

[15] Fischler, M.A., Bolles, R.C., 1981. Random sample consensus: a paradigm for model fitting with applications to image analysis and automated cartography. Communications of the ACM 24, 381–395.

[16] Flitton, G., Breckon, T., Megherbi Bouallagu, N., 2010. Object Recognition using 3D SIFT in Complex CT Volumes. Proceedings of British Machine Vision Conference , 11.1–12.

[17] Flitton, G., Breckon, T.P., Megherbi, N., 2013. A comparison of 3D interest point descriptors with application to airport baggage object detection in complex CT imagery. Pattern Recognition 46, 2420–2436. doi:10.1016/j.patcog.2013.02.008.

[18] Hing, C.B., Smith, T.O., Donell, S., 2011. Surgical versus non-surgical interventions for treating patellar dislocation. Cochrane Database Systematic Reviews 11.

[19] Keefe, D.F., Ewert, M., Ribarsky, W., Chang, R., 2009. Interactive Coordinated Multiple-View Visualization of Biomechanical Motion Data. IEEE Transactions on Visualization and Computer Graphics 15, 1383–1390.

[20] König, A.H., Doleisch, H., Gröller, E., 1999. Multiple views and magic mirrors-fMRI visualization of the human brain. Technical Report. Institute of Computer Graphics and Algorithms, Vienna University of Technology.

[21] Krekel, P.R., Botha, C.P., Valstar, E.R., de Bruin, P.W., Rozing, P.M., Post, F.H., 2006. Interactive simulation and comparative visualisation of the bone-determined range of motion of the human shoulder. Proceedings of Simulation and Visualization , 275–288.

[22] Krekel, P.R., Valstar, E.R., De Groot, J., Post, F.H., Nelissen, R.G.H.H., Botha, C.P., 2010. Visual Analysis of Multi-Joint Kinematic Data. Computer Graphics Forum 29, 1123–1132.

[23] Lindeberg, T., 1994. Scale-space theory: A basic tool for analysing structures at different scales. Journal of applied statistics 21, 225–270.

[24] Lowe, D.G., 1999. Object recognition from local scale-invariant features. The Proceedings of the Seventh IEEE International Conference on Computer Vision 2, 1150–1157.

[25] Lowe, D.G., 2004. Distinctive image features from scale-invariant keypoints. International Journal of Computer Vision 60, 91–110.

[26] Manal, K., Chang, C.C., Hamill, J., Stanhope, S.J., 2005. A three-dimensional data visualization technique for reporting movement pattern deviations. Journal of Biomechanics 38, 2151–2156.

[27] Manal, K., Stanhope, S.J., 2004. A novel method for displaying gait and clinical movement analysis data. Gait & Posture 20, 222–226.

[28] Mann, H.B., Whitney, D.R., 1947. On a test of whether one of two random variables is stochastically larger than the other. The annals of mathematical statistics 18, 50–60.

[29] McNally, E.G., Ostlere, S.J., Pal, C., Phillips, A., Reid, H., Dodd, C., 2000. Assessment of patellar maltracking using combined static and dynamic MRI. European Radiology 10, 1051–1055.

[30] Mikolajczyk, K., Tuytelaars, T., Schmid, C., Zisserman, A., Matas, J., Schaffalitzky, F., Kadir, T., Van Gool, L., 2005. A comparison of affine region detectors. International Journal of Computer Vision 65, 43–72.

[31] Ni, D., Qu, Y., Yang, X., Chui, Y.P., Wong, T.T., Ho, S.S., Heng, P.A., 2008. Volumetric Ultrasound Panorama Based on 3D SIFT. Proceedings of the 11th International Conference on Medical Image Computing and Computer-Assisted Intervention, Part II , 52–60.

[32] Nietosvaara, Y., Aalto, K., Kallio, P.E., 1994. Acute Patellar Dislocation in Children: Incidence and Associated Osteochondral Fractures. Journal of Pediatric Orthopaedics 14, 513.

[33] Paganelli, C., Peroni, M., Pennati, F., Baroni, G., Summers, P., 2012. Scale Invariant Feature Transform as feature tracking method in 4D imaging: A feasibility study. Engineering in Medicine and Biology Society (EMBC), Annual International Conference of the IEEE , 6543–6546.

[34] Powers, C.M., Shellock, F.G., Pfaff, M., 1998. Quantification of patellar tracking using kinematic MRI. Journal of Magnetic Resonance Imaging 8, 724–732. doi:10.1002/jmri.1880080332.

[35] Pronost, N., Sandholm, A., Thalmann, D., 2011. A visualization framework for the analysis of neuromuscular simulations. The Visual Computer: International Journal of Computer Graphics 27.

[36] Rasch, H., Falkowski, A.L., Forrer, F., Henckel, J., Hirschmann, M.T., 2013. 4D-SPECT/CT in orthopaedics: a new method of combined quantitative volumetric 3D analysis of SPECT/CT tracer uptake and component position measurements in patients after total knee arthroplasty. Skeletal Radiology 42, 1215–1223. doi:10.1007/s00256-013-1643-2.

[37] Rhee, S.J., Pavlou, G., Oakley, J., Barlow, D., Haddad, F., 2012. Modern management of patellar instability. International Orthopaedics 36, 2447–2456. doi:10.1007/s00264-012-1669-4.

[38] Scovanner, P., Ali, S., Shah, M., 2007. A 3-dimensional SIFT descriptor and its application to action recognition. Proceedings of the 15th international conference on Multimedia , 357–360.

[39] Shams, R., Kennedy, R.A., 2007. Efficient histogram algorithms for NVIDIA CUDA compatible devices, in: Proc. Int. Conf. on Signal Processing and Communications Systems (ICSPCS), Gold Coast, Australia. pp. 418–422.

[40] Shellock, F.G., Mink, J.H., Deutsch, A.L., Foo, T.K., Sullenberger, P., 1993. Patellofemoral joint: identification of abnormalities with active-movement, "unloaded" versus "loaded" kinematic MR imaging techniques. Radiotherapy and Oncology 188, 575–578.

[41] Smith, T.O., Davies, L., Toms, A.P., Hing, C.B., Donell, S.T., 2010. The reliability and validity of radiological assessment for patellar instability. A systematic review and meta-analysis. Skeletal Radiology 40, 399–414. doi:10.1007/s00256-010-0961-x.

[42] Toews, M., Wells, III, W.M., 2012. Efficient and Robust Model-to-Image Alignment using 3D Scale-Invariant Features. Medical Image Analysis 17, 271–82.

[43] Ward, S.R., Shellock, F.G., Terk, M.R., Salsich, G.B., Powers, C.M., 2002. Assessment of patellofemoral relationships using kinematic MRI: Comparison between qualitative and quantitative methods. Journal of Magnetic Resonance Imaging 16, 69–74.

[44] Whittle, M., 2007. Gait analysis: an introduction. Butterworth-Heinemann Medical.

[45] Yu, T.H., Woodford, O.J., Cipolla, R., 2012. A Performance Evaluation of Volumetric 3D Interest Point Detectors. International Journal of Computer Vision 102, 180–197.